

This is the accepted manuscript made available via CHORUS. The article has been published as:

Band Jahn-Teller structural phase transition in $\text{Y}_{\{2\}}\text{In}$

E. Svanidze, C. Georgen, A. M. Hallas, Q. Huang, J. M. Santiago, J. W. Lynn, and E. Morosan

Phys. Rev. B **97**, 054111 — Published 23 February 2018

DOI: [10.1103/PhysRevB.97.054111](https://doi.org/10.1103/PhysRevB.97.054111)

Band Jahn-Teller Structural Phase Transition in Y_2In

E. Svanidze,^{1,*} C. Georgen,¹ A. M. Hallas,¹ Q. Huang,² J. M. Santiago,¹ J. W. Lynn,² and E. Morosan¹

¹*Department of Physics and Astronomy and Rice Center for Quantum Materials, Rice University, Houston, TX, 77005 USA*

²*NIST Center for Neutron Research, National Institute of Standards and Technology, MD 20899, USA*

(Dated: February 13, 2018)

The number of paramagnetic materials that undergo a structural phase transition is rather small, which can perhaps explain the limited understanding of the band Jahn-Teller mechanism responsible for this effect. Here we present a structural phase transition observed in paramagnetic Y_2In at temperature $T_0 = 250 \pm 5$ K. Below T_0 , the high-temperature hexagonal $P6_3/mmc$ phase transforms into the low-temperature orthorhombic $Pnma$ phase. This transition is accompanied by an unambiguous thermal hysteresis of about 10 K, observed in both magnetic susceptibility $M/H(T)$ and resistivity $\rho(T)$, indicating a first order transition. Band structure calculations suggest a band Jahn-Teller mechanism, during which the degeneracy of electron bands close to the Fermi energy is broken. We establish that this structural phase transition does not have a magnetic component; however, the possibility of a charge density wave formation has not been eliminated.

I. INTRODUCTION

A structural phase transition can be driven by a number of parameters – temperature [1–6], pressure [7], chemical composition [8, 9], or magnetic field [10, 11]. When the driving parameter is temperature, the transition typically occurs from a higher to a lower symmetry [12]. This is illustrated by a large number of austenite-martensite structural phase transitions, in which the high-temperature cubic phase is transformed into a low-temperature tetragonal one [4]. If the symmetry of two phases is different, the structural phase transition is likely to be first order, resulting in a discontinuous volume change. A reliable indicator of a first order phase transition is the presence of hysteresis [13–15]. For temperature-induced transitions, the high- and low-temperature phases coexist in the region corresponding to the width of the hysteresis – in some materials this region can be as small as a fraction of a Kelvin [16] while in others it can reach several hundreds of Kelvin [3, 4, 6, 17]. Materials with wide thermal hystereses are frequently used as a basis for shape-memory devices [14].

Structural phase transitions are frequently accompanied by various phenomena. In magnetic compounds, structural phase transitions often accompany the magnetic order [1, 2, 5, 9, 18]. In metals, charge transfer between various atoms can result in a change of valence, *e.g.* Mn- and Fe-based materials [14, 19], that could lead to a metal-insulator transition [20]. The formation of a spin [21] or charge [22–24] density wave has also been associated with structural distortions. The origin of a structural instability in transition metals has been attributed to either a cooperative Jahn-Teller distortion (in systems with local moments) or a band Jahn-Teller effect (in systems without local moments) [12, 25, 26]. In the

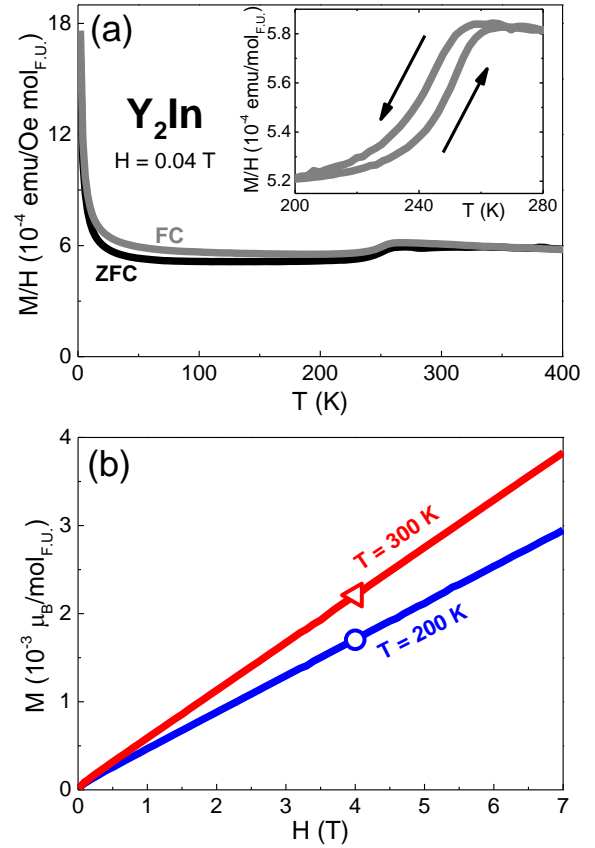


FIGURE 1. (a) The zero field-cooled (black line) and field-cooled (gray line) temperature-dependent magnetic susceptibility $M/H(T)$ data of Y_2In , measured in $H = 0.04$ T. Inset: the thermal hysteresis around the $T_0 = 250 \pm 5$ K transition. [Note: $1 \text{ emu}/(\text{mol}_{F.U.} \text{ Oe}) = 4\pi \cdot 10^{-6} \text{ m}^3/\text{mol}$] (b) Magnetization isotherms $M(H)$, measured at $T = 200$ K (circle), and 300 K (triangle).

* Present address: Max Planck Institute for Chemical Physics.

band Jahn-Teller model, the lattice distortion breaks the degeneracy of the electron bands in the vicinity of the Fermi energy, which results in a redistribution of electrons

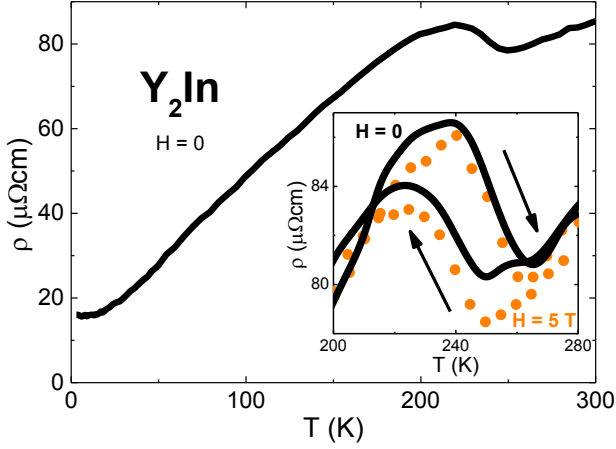


FIGURE 2. The temperature-dependent resistivity $\rho(T)$ of Y_2In in $H = 0$. Inset: the thermal hysteresis in $H = 0$ (line) and $H = 5$ T (symbols).

between these bands, lowering the free energy [26]. The occurrence of a structural phase transition within the band Jahn-Teller model is suggested to arise in compounds for which there exists a sharp d -electron dominated peak close to the Fermi energy, E_F , which is either flattened or split into two peaks as a result of a structural phase transition [27–29]. Experimental realizations of this model include YCu [30] and LaCd [28].

While the majority of the $R_2\text{In}$ compounds crystallize in the hexagonal $P6_3/mmc$ structure [31, 32], some are known to occur in the $Pnma$ space group [33, 34]. This, together with a large peak in the density of states close to the Fermi energy $\text{DOS}(E_F)$ [35], suggests the possibility of a band Jahn-Teller transition in Y_2In . In this paper, we present evidence for a structural phase transition from the high-temperature $P6_3/mmc$ to a low-temperature $Pnma$ phase in Y_2In . The transition is signaled by a step in the temperature-dependent susceptibility $M/H(T)$ as well as resistivity $\rho(T)$ around $T_0 = 250 \pm 5$ K. In both measurements, a well-pronounced hysteresis of about 10 K suggests that the transition is first order, consistent with an abrupt volume change. Band structure calculations reveal the expected flattening of the d -electron peak in the $\text{DOS}(E_F)$.

II. EXPERIMENTAL METHODS

Several polycrystalline samples were synthesized by arc-melting Y (Hefa Rare Earths, 99.9%) and In (Alfa Aesar, 99.9995%) in ratios ranging from 1.8:1 to 2.3:1 with mass losses of no more than 0.5%. The arc-melted buttons were then wrapped in Ta foil and annealed at 950 °C, 850 °C, and 750 °C for 96 hours each. Both annealed and non-annealed samples are extremely air sensitive, similar to other R -In compounds [36]. All thermodynamic

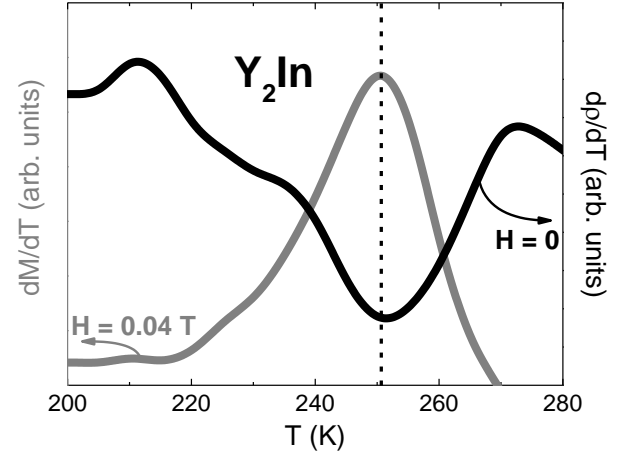


FIGURE 3. The transition temperature $T_0 = 250 \pm 5$ K, determined from the derivatives of susceptibility $d(M/H(T))/dT$ ($H = 0.04$ T, gray line, left axis) and resistivity $d\rho(T)/dT$ ($H = 0$, black line, right axis).

and transport measurements show the sharpening of the features associated with the transition upon annealing, and a dependence of the transition width and magnitude with the exact Y:In composition. All data presented here are for the Y:In = 2.2:1 annealed specimens, which showed the sharpest transition and the highest step in magnetization and resistivity. Powder neutron and x-ray diffraction at room temperature confirm the known $P6_3/mmc$ structure of Y_2In . Additional temperature-dependent neutron diffraction data were collected on the BT-1 powder diffractometer at the NIST Center for Neutron Research. Collimators of 15', 20' and 7' were used before and after the Cu (311) monochromator ($\lambda = 1.5401$ Å) and after the sample, respectively, and data were collected in steps of 0.05° in the 2θ range of 3° to 168° . The results of the Rietveld structural refinements with the FullProf software of the data below ($T = 200$ K) and above ($T = 300$ K) the structural phase transition are summarized in Table I. Due to high air sensitivity of the samples, diffraction data were collected on a powder sample sealed under an inert atmosphere in a Pyrex tube. Complementary powder x-ray diffraction measurements using Cu K_α radiation ($\lambda = 1.5401$ Å) were carried out at several temperatures between 200 K and 300 K in a Bruker diffractometer equipped with a liquid nitrogen cooled sample stage.

Temperature- and field-dependent DC magnetization measurements were performed in a Quantum Design (QD) Magnetic Property Measurement System for temperatures between 1.8 K and 400 K, and for applied magnetic fields up to 7 T. Specific heat was measured from 2 K to 100 K in a QD Physical Property Measurement System (PPMS). DC resistivity measurements from 2 K to 300 K were carried out using the standard four-probe method in the QD PPMS in $H = 0$.

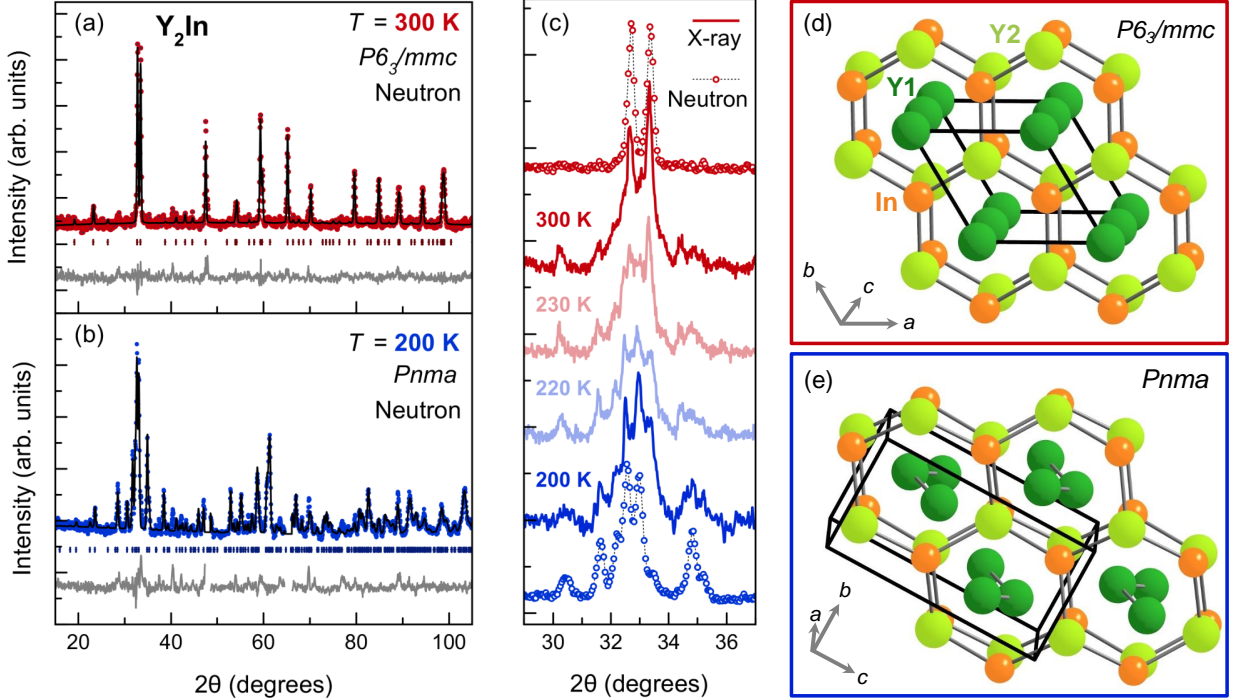


FIG. 4. Neutron diffraction patterns of Y_2In (symbols) for (a) $T = 300$ K and (b) $T = 200$ K. The data were fit (black line) with (a) $P6_3/mmc$ and (b) $Pnma$ space groups, with calculated peak positions represented by the vertical symbols. The difference between measured and fit data is shown as a gray line. (c) Evolution of the x-ray diffraction pattern (solid lines) between 200 K and 300 K compared with the neutron data (symbols). The high- and low-temperature crystal structures are shown in panels (d) $P6_3/mmc$ and (e) $Pnma$, with the unit cell outlined in black.

Band structure calculations were performed using the full-potential linearized augmented plane-wave method implemented in the *WIEN2K* package [37, 38]. The PBE-GGA exchange-correlation potential was used and a $10 \times 10 \times 10$ grid was used to sample the k -points in the Brillouin zone.

III. RESULTS AND DISCUSSION

The magnetic properties of $R_2\text{In}$ compounds are diverse, ranging from antiferromagnets ($R = \text{Gd}$, Tb and Dy) and ferromagnets ($R = \text{Ho}$, Er , Tm) to weak diamagnets ($R = \text{Sm}$, Yb , Eu) [39]. The magnetic susceptibility of Y_2In was previously reported to be temperature-independent, and no transitions were observed in the temperature range between 4.2 K and 300 K [39]. By contrast, our temperature-dependent magnetization data for Y_2In reveal a step around $T_0 = 250$ K (Fig. 1(a)). The slight upturn in the low-temperature susceptibility data points towards the presence of a small magnetic impurity, which amounts to 0.003 % Gd. A well-pronounced thermal hysteresis with a width of about 10 K, shown in the inset of Fig. 1(a), suggests that the T_0 transition is first order [13–15]. Such a step has previously been observed in the magnetic susceptibility of a number of

materials with structural phase transitions [1–6], some of which are accompanied by magnetic spin reorientations [18, 40]. In order to check whether or not the transition has a magnetic component, field-dependent magnetization isotherms were measured at temperatures below and above the transition, as shown in Fig. 1(b). Both the $T = 200$ K (blue circle) and $T = 300$ K (red triangle) isotherms appear to be paramagnetic.

The temperature-dependent resistivity data (Fig. 2) support the possibility of a structural phase transition around $T_0 = 250 \pm 5$ K. A hysteretic jump around T_0 is observed in $\rho(T)$ (Fig. 2), slightly broader ($\Delta T \sim 10$ K) than the $M/H(T)$ hysteresis. The resistivity enhancement associated with the transition $\Delta\rho(T)/\rho(T) \approx 9\%$ is large and comparable to what had been observed for other structural phase transitions [1, 2, 16]. The small residual resistivity ratio $\text{RRR} = \rho(300 \text{ K})/\rho(2 \text{ K}) = 5$ can be attributed to the polycrystalline sample form. From the inset of Fig. 2, it is clearly seen that both the transition temperature T_0 and the thermal hysteresis width are essentially unchanged with field, confirming the lack of a magnetic component. A better estimate of T_0 is available from combined derivatives of susceptibility $d(M/H(T))/dT$ (Fig. 3, gray line, left axis) and resistivity $d\rho(T)/dT$ (Fig. 3, black line, right axis), which give $T_0 = 250 \pm 5$ K, where the uncertainty corresponds to the

TABLE I. Summary of parameters for the two Y_2In phases.

Space Group	Lattice parameters			Volume (\AA^3)	χ (high T , low H) (10^{-4} emu/mol _{F.U.})	$\chi_0 = \mu_B^2 \text{DOS}(E_F)$ (10^{-4} emu/mol _{F.U.})
	a (\AA)	b (\AA)	c (\AA)			
$P6_3/mmc$	5.3599(2)	5.3599(2)	6.7647(3)	168.57	$\chi(300 \text{ K}, 0.04 \text{ T}) = 5.8$	7.0
$Pnma$	6.7486(4)	5.1426(4)	9.7382(7)	337.97	$\chi(200 \text{ K}, 0.04 \text{ T}) = 5.2$	5.9

width of the hysteresis.

To further examine the nature of the step-like transition in Y_2In , structural analysis of the powder neutron diffraction patterns was performed at temperatures above ($T = 300 \text{ K}$, Fig. 4(a)) and below ($T = 200 \text{ K}$, Fig. 4(b)) T_0 . At high-temperature, Y_2In forms in the hexagonal $P6_3/mmc$ structure (Fig. 4(d)), consistent with previous reports [31, 32]. Upon cooling through the $T_0 = 250 \pm 5 \text{ K}$ transition, the structure changes to the orthorhombic $Pnma$ (Fig. 4(e)), which has not been reported previously. The temperature evolution of this structural transition was studied with powder x-ray diffraction (Fig. 4(c)). As the wavelengths of the neutron and x-ray diffraction measurements are equivalent, the peak positions can be directly compared at $T = 300 \text{ K}$ and $T = 200 \text{ K}$, showing good agreement. However, the relative peak intensities can not be directly compared, due to the difference in the scattering interaction. At $T = 300 \text{ K}$, there are two prominent Bragg peaks between 32° and 34° , which are indexed as (102) and (110) in the $P6_3/mmc$ space group. Cooling through the symmetry reducing structural transition, many new Bragg peaks emerge, including an intense reflection at 33° , which is indexed as (211) within the $Pnma$ space group. The x-ray diffraction measurements at $T = 230 \text{ K}$ and $T = 220 \text{ K}$ show coexistence of Bragg reflections from both the high- and low-temperature phases, consistent with the interval of hysteresis shown in Fig. 1(a).

The nature of the structural transition in Y_2In can be understood by comparing the crystal structures presented in Fig. 4(d) and (e) of the high-temperature hexagonal ($P6_3/mmc$) and low-temperature orthorhombic ($Pnma$) phases, respectively. In both structures the indium atoms (orange) occupy a single crystallographic site and the yttrium atoms occupy two crystallographic sites (Y1, dark green and Y2, light green). In the hexagonal case, the structure can be visualized as Y1 chains along the c -axis, enclosed by a honeycomb of In and Y2 within the ab plane. Within the honeycomb lattice, the Y2–In distance is 3.11 \AA , while the adjacent honeycomb layers are separated by 3.39 \AA . In the orthorhombic structure, the Y1 atoms are displaced into a buckled chain, leading to an increased Y1–Y1 distance. The honeycomb of In and Y2 is also distorted, primarily along the a -axis, with the Y1–In separation alternating between 2.73 \AA and

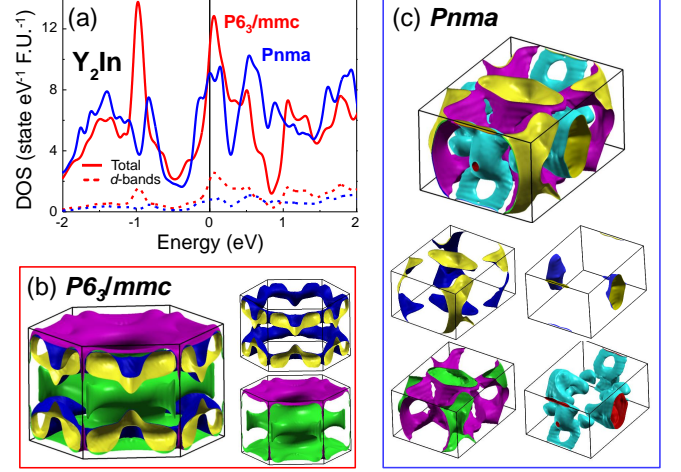


FIGURE 5. (a) The total (solid line) and d -electron (dashed line) non-magnetic density of states for the $Pnma$ (blue line) and the $P6_3/mmc$ (red line) phases of Y_2In . Fermi surface plots for the (b) $P6_3/mmc$ and (c) $Pnma$ phases of Y_2In .

4.02 \AA .

The experimental evidence for the structural transition at T_0 motivated band structure calculations, which are shown in Fig. 5(a). The $\text{DOS}(E_F)$ is larger for the high-temperature phase than the low-temperature phase. This is consistent with the observed drop in the Pauli susceptibility, with the respective χ_0 values listed in Table I. The d -electron contribution to the DOS shows a peak for the high-temperature phase, which then flattens out in the low-temperature phase (dashed lines). Both the total and partial DOS are similar to those calculated for YCu [30] and LaCd [28], two materials that undergo structural phase transition driven by the band Jahn-Teller mechanism. The number of bands contributing to the $\text{DOS}(E_F)$ is two for the high-temperature phase and four for the low-temperature phase, consistent with a lowered free energy (Fig. 5(b) and (c)).

It is important to note that the structural phase transition in Y_2In can be accompanied by formation of a charge density wave. However, a definitive analysis is only possible for single crystals which are currently not available.

IV CONCLUSIONS

It was found that Y_2In exhibits a structural phase transition at $T_0 = 250 \pm 5$ K, as evidenced by crystallographic analysis, magnetization, and resistivity data. The phase transition from a high-temperature hexagonal $P6_3/mmc$ to a low-temperature orthorhombic $Pnma$ phase is accompanied by a large thermal hysteresis of about 10 K, indicating that this transition is first order. Based on the band structure calculations, this structural phase transition can likely be attributed the band Jahn-Teller effect. The possibility of an accompanying charge density wave formation has not been ruled out and is left to a future study.

ACKNOWLEDGMENTS

The work at Rice (ES, CG, AMH, JMS, and EM) was supported by NSF DMR-1506704. The identification of any commercial product or trade name does not imply endorsement or recommendation by the National Institute of Standards and Technology.

-
- [1] N. Ni, S. Nandi, A. Kreyssig, A. Goldman, E. D. Mun, S. L. Bud'ko, and P. C. Canfield, *Physical Review B* **78**, 014523 (2008).
 - [2] G. Wu, H. Chen, T. Wu, Y. L. Xie, Y. J. Yan, R. H. Liu, X. F. Wang, J. J. Ying, and X. H. Chen, *Journal of Physics: Condensed Matter* **20**, 422201 (2008).
 - [3] H. Balster, H. Ihrig, a. Kockel, and S. Methfessel, *Zeitschrift fur Physik B* **21**, 241 (1975).
 - [4] H. Kadomatsu, Y. Kawanishi, M. Kurisu, T. Tokunaga, and H. Fujiwara, *Journal of the Less Common Metals* **141**, 29 (1988).
 - [5] M. Tegel, M. Rotter, V. Weiss, F. M. Schappacher, R. Pottgen, and D. Johrendt, *Journal of Physics: Condensed Matter* **452201**, 11 (2008).
 - [6] E. L. Semenova and Y. Kudryavtsev, *Journal of Alloys and Compounds* **203**, 165 (1994).
 - [7] M. Kurisu, *Journal of the Physical Society of Japan* **56**, 4064 (1987).
 - [8] K. Yagasaki, Y. Uwatoko, Y. Fadena, H. Fujii, and T. Okamoto, *Journal of Physics F* **15**, 651 (1985).
 - [9] H. Ihrig and W. Lohmann, *Journal of Physics F* **7**, 1957 (1977).
 - [10] A. Asamitsu, Y. Moritomo, Y. Tomioka, T. Arima, and Y. Tokura, *Nature* **373**, 407 (1995).
 - [11] A. Asamitsu, Y. Moritomo, R. Kumai, Y. Tomioka, and Y. Tokura, *Physical Review B* **54**, 1716 (1996).
 - [12] K. A. Muller and H. Thomas, *Structural Phase Transitions* (Springer-Verlag, 1991).
 - [13] Y. Mnyukh, *American Journal of Condensed Matter Physics* **3**, 25 (2013).
 - [14] S. Ohkoshi, T. Matsuda, H. Tokoro, and K. Hashimoto, *Chemistry of Materials* **17**, 81 (2005).
 - [15] D. G. Thomas and L. A. Staveley, *Journal of the Chemical Society* **573**, 2572 (1951).
 - [16] J. Q. Yan, S. Nandi, B. Saparov, P. Čermák, Y. Xiao, Y. Su, W. T. Jin, A. Schneidewind, T. Brückel, R. W. McCallum, T. A. Lograsso, B. C. Sales, and D. G. Mandrus, *Physical Review B* **91**, 024501 (2015).
 - [17] Y. Gefen and M. Rosen, *Scripta Metallurgica* **14**, 645 (1980).
 - [18] S. Li, C. De La Cruz, Q. Huang, Y. Chen, J. W. Lynn, J. Hu, Y. L. Huang, F. C. Hsu, K. W. Yeh, M. K. Wu, and P. Dai, *Physical Review B* **79**, 054503 (2009).
 - [19] O. Jung, D. Jo, Y. Lee, B. Conklin, and C. G. Pierpont, *Inorganic Chemistry* **36**, 19 (1997).
 - [20] T. Furubayashi, T. Matsumoto, T. Hagino, and S. Nagata, *Journal of the Physical Society of Japan* **63**, 3333 (1994).
 - [21] T. R. McGuire and C. J. Kriessman, *Physical Review* **85**, 452 (1952).
 - [22] C. Lue, Y. K. Kuo, F. Hsu, H. Li, H. Yang, P. Fodor, and L. Wenger, *Physical Review B* **66**, 10 (2002).
 - [23] G. Grüner, *Reviews of Modern Physics* **60**, 1129 (1988).
 - [24] N. S. Sangeetha, A. Thamizhavel, C. V. Tomy, S. Basu, A. M. Awasthi, P. Rajak, S. Bhattacharyya, S. Ramakrishnan, and D. Pal, *Physical Review B* **91**, 205131 (2015).
 - [25] J. N. Lalena and D. A. Cleary, *Principles of Inorganic Materials Design* (Wiley-Interscience, 2005).
 - [26] P. J. Brown, A. Y. Bargawi, J. Crangle, K. U. Neumann, and K. R. Ziebeck, *Journal of Physics: Condensed Matter* **11**, 4715 (1999).
 - [27] S. K. Ghatak, D. K. Ray, and C. Tannous, *Physical Review B* **18**, 5379 (1978).
 - [28] S. Asano and S. Ishida, *Journal of the Physical Society of Japan* **54**, 4241 (1985).
 - [29] S. Fujii, S. Ishida, and S. Asano, *Journal of the Physical Society of Japan* **58**, 3657 (1989).
 - [30] Y. J. Shi, Y. L. Du, G. Chen, and G. L. Chen, *Physics Letters A* **368**, 495 (2007).
 - [31] E. Franceschi, *Journal of the Less-Common Metals* **37**, 157 (1974).
 - [32] A. Palenzona, *Journal of the Less-Common Metals* **16**, 379 (1968).
 - [33] M. L. Fornasini and S. Cirafici, *Zeitschrift fuer Kristallographie* **190**, 295 (1990).
 - [34] O. D. McMasters, C. L. Nipper, and K. A. Gschneidner, *Journal of Less-Common Metals* **23**, 253 (1970).
 - [35] S. Curtarolo, W. Setyawan, S. Wang, J. Xue, K. Yang, R. H. Taylor, L. J. Nelson, G. L. W. Hart, S. Sanvito, M. Buongiorno-Nardelli, N. Mingo, and O. Levy, *Computational Materials Science* **58**, 227 (2012).
 - [36] E. Franceschi, *Journal of the Less-Common Metals* **37**, 157 (1974).
 - [37] P. K. Blaha, K. Schwarz, G. Madsen, D. Kvasnicka, and J. Luitz, *WIEN2K package* <http://www.wien2k.at> (2001).
 - [38] J. P. Perdew, K. Burke, and M. Ernzerhof, *Physical Review Letters* **77**, 3865 (1996).
 - [39] H. Gamari-Seale, T. Anagnostopoulos, and J. K. Yakinthos, *Journal of Applied Physics* **50**, 434 (1979).
 - [40] A. Yamada and M. Tanaka, *Materials research bulletin* **30**, 715 (1995).